WARSAW UNIVERSITY OF TECHNOLOGY Index 351733
FACULTY OF CIVIL ENGINEERING
COMMITTEE FOR CIVIL AND WATER ENGINEERING
POLISH ACADEMY OF SCIENCES ISSN 1230-2945

DOI: 10.24425/ace.2021.137184

ARCHIVES OF CIVIL ENGINEERING

Vol. LXVII ISSUE 2 2021

s. 537–550

Research paper

Experimental and theoretical research on large-diameter rock-socketed pile embedded depth

Yanfeng Li[1], Jihe Zhao[2], Ying Xiong[3], Qinghe Wang[4]

Abstract: A theoretical formula for large-diameter rock-socket depth is developed to support pail embedding in a large bridge pile foundation project. There is a horizontal additional stress concentration at the place where the soil around the rock-socketed pile meets the soil layer under the horizontal load. When the rock-socketed tip stress and bending moment of the pile are relatively small, the pile shows favourable embedment effect and the pile foundation can be considered safe. The function curve of soil resistance around the pile under the action of horizontal force was obtained by finite element analysis. The force characteristics reveal the depth of the large-diameter rock-socketed pile under the horizontal load. As the rock-socketed pile rotates under the action of horizontal force, the rock mass resistance around the pile changes according to the cosine. The distribution of pile-side soil resistance is proportional to the displacement and distributed according to the sine. A comprehensive correction coefficient of pile shaft resistance β is introduced to deduce the theoretical formula of the depth h_r of the large-diameter rock-socketed pile embedded in the bedrock. It is verified through both experiments and numerical analysis.

Keywords: Horizontal loading test; finite element model; load transfer; ultimate bearing capacity; rock socket depth

[1] Prof., PhD., School of Transportation Engineering, Shenyang Jianzhu University, Shenyang 110168, China, e-mail: lyfneu@126.com, ORCID: https://orcid.org/0000-0003-2153-7934

[2] DSc., School of Transportation Engineering, Shenyang Jianzhu University, Shenyang 110168, China, e-mail: zjh321814@163.com, ORCID: https://orcid.org/0000-0001-7245-4069

[3] DSc., School of Transportation Engineering, Shenyang Jianzhu University, Shenyang 110168, China, e-mail: 811633834@qq.com, ORCID: https://orcid.org/0000-0001-9720-7048

[4] Prof., PhD., School of Transportation Engineering, Shenyang Jianzhu University, Shenyang 110168, China, e-mail: wangqinghe@sjzu.edu.cn, ORCID: https://orcid.org/0000-0002-1530-4555

1. Introduction

Advanced bridge construction techniques have made newly constructed bridges across rivers and valleys increasingly common in recent decades. Rock-socketed piles are widely used in the construction of bridge foundations due to their high bearing capacity and small settlement. The bearing capacity of a rock-socketed pile is jointly assumed by pile tip resistance and pile lateral friction resistance. Many previous scholars have conducted theoretical analyses, field tests, and laboratory model tests on the bearing capacity of rock-socketed piles [1] [2] [3] [4] [5]. Field test monitoring data has shown that strong rock and soil at the pile tip can strengthening the pile side resistance [6] [7]. Hole wall roughness is also known to affect the ultimate bearing capacity of soft rock-socketed piles [8]. The pile-rock interface experiences sliding dilatancy and shear slip [9]; the pile-rock interface roughness can be assumed to be destroyed during shearing movement [10] in the form of a direct shear fracture from the root [11] [12]. The cementation effect and initial stress of concrete side of pile have also been considered empirically.

There has been a great deal of research to date on the vertical bearing mechanism of the pile foundation[13] [14] [15] [16] [17], but relatively few analyses of the horizontal bearing mechanism of large-diameter rock-socketed piles. As the self-weight and moving load of bridge superstructures continue to increase, their pile foundation requirements grow increasingly stringent. Modern pile foundation engineering designs require that additional rock-socketed piles be considered to bear horizontal loads. The force mechanism of the pile foundation under the horizontal load of a rock-socketed pile, and the resistance of the soil around the pile, were taken as the research object in this study. A finite element theory analysis was conducted based on horizontal loading test results. The force of the pile and the soil under the horizontal load of the rock-socketed pile were used to determine the depth of rock socketing.

ABAQUS finite element software was also used to conduct a numerical simulation of horizontal load on the large diameter rock-socketed piles of a solid bridge. The influence factors of rock-socketed pile horizontal stress were taken into consideration to construct a comparative model of the change trend of soil resistance around the pile under the action of horizontal force. The experimental and numerical simulation results were compared to determine the force characteristics of rock-socketed piles, particularly, the depth of the large-diameter rock-socketed pile with large diameter under horizontal load. A comprehensive correction coefficient of pile shaft resistance, β was established to deduce the theoretical formula of the depth h_r of the large-diameter rock-socketed pile embedded

in the bedrock. The results were verified through both experiments and numerical analysis. This work may have certain reference significance for similar projects.

2. Field test of rock-socketed pile under horizontal load

The diameter of both pile I and pile II subjected to the field test are 2.2 m. The pile length is 12 m, which is the design value for rock-socketed piles. The rock-socket depth is about 3 times the pile diameter. The bending moment distribution of rock-socketed pile and the stress condition of pile bottom under various loads were obtained via horizontal loading test. The stress deformation mechanism of the large-diameter rock-socketed pile under horizontal loads was determined accordingly.

Fig. 1. Lifting reinforcing cage

Fig. 2. Pile foundation concrete pouring completed

2.1. Test plan

The horizontal loading point is at the center of the pile tie beam. The riverbed scour should be considered; the distance between the loading point and the bedrock roof is 4 m in this case. To achieve 100% test efficiency, horizontal loading force was defined as $P_{\max} \approx M_H / h = F_u$, where $P_{\max}$ has exceeded the horizontal bearing capacity of the pile. The bearing capacity of the pile should also be considered. The temporary horizontal loading force $0.5F_u \le P_{\max} < F_u$, with a test efficiency of 82%, can be used to simulate the stress state of a pile foundation after the bridge is completed. The test layout is shown in Fig. 3.

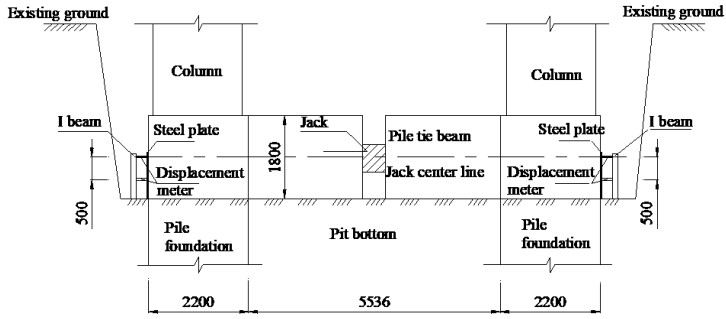

Fig. 3. Test elevation

The horizontal bearing capacity of the rock-socketed pile was estimated to be F=1600kN. The test was run using a cyclic loading and unloading scheme. The horizontal load was applied at 13 levels each with a load increment P of 100kN.

In this test, 108 concrete strain gauges and 68 steel bar strain gauges were installed on the main steel bars in the test pile. The specific locations are shown in Fig. 4. Four concrete strain gauges and four steel strain gauges were arranged on the pile. The bending moment value of the pile section cannot be read directly, so it was approximated by the readings of the concrete and steel bar strain gauges placed inside the pile [18] [19]. The bending moment at each section of the pile was then calculated.

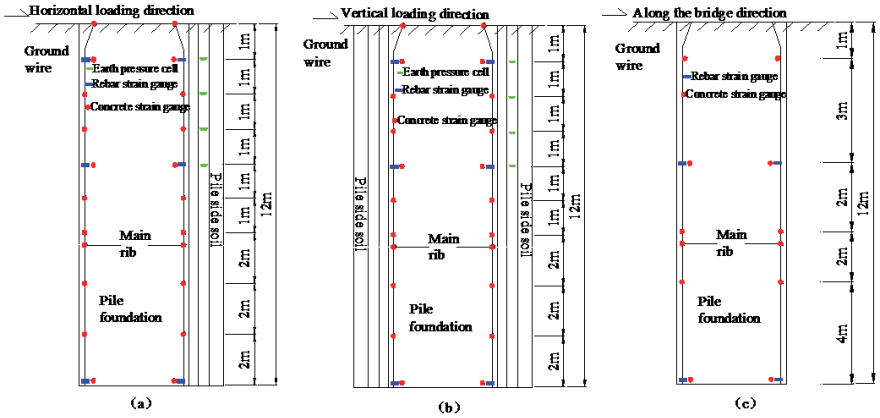

Fig. 4. Sensor layout: (a) Horizontal load direction sensor position; (b) Sensor position perpendicular to loading direction; (c) Along bridge sensor.

The distribution of soil resistance on the side of pile is complicated. There are many factors that influence the measurement of soil pressure force[20]. The most direct approach is to bury an earth

pressure cell on the side of the pile [21] [22]. In this test, a total of 24 earth pressure cells were used to measure the soil resistance values on the side of the pile at different depths. The locations of the soil resistance cells are shown in Fig.5.

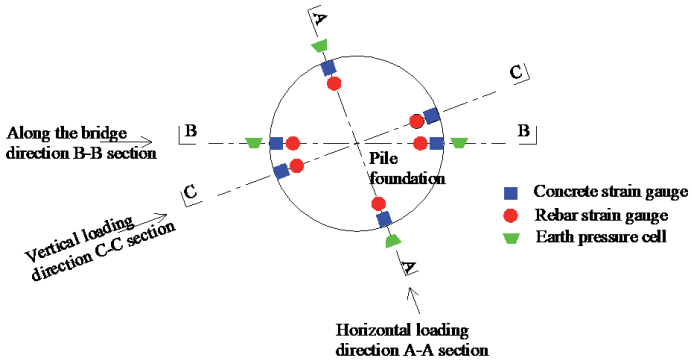

Fig. 5. Earth pressure box layout

During the test, the jack loading force was applied as horizontally as possible on the central axis of the pile. The displacement measuring rod and the generated displacement were imposed in the same direction to ensure that the rod was sufficiently flexible. The track of the measured point was kept parallel to the central axis of the sensor rod and the surface of the measuring point was kept smooth and flat.

2.2. Analysis of test results

In the initial stage of loading, the horizontal load on pile foundation is relatively low. The linear variation relationship of each parameter is small and increases uniformly. The horizontal load of the pile foundation is borne by the resistance of the upper soil, and the soil around the pile is still in the elastic compression stage before reaching the limit state; the soil deformation is experiencing an elastic change. As the horizontal load of the test pile increases, the bearing capacity of the pile foundation increases and the shape variable increases. The load transferred by the test pile to the upper soil layer is strengthened as the upper soil layer gradually reaches the limit state. The soil mass produces plastic yield, then the horizontal load received by the soil layer begins to transfer to the deeper rock layer. The upper soil layer and the lower rock layer bear the horizontal load together. When the upper soil layer reaches the ultimate bearing state, the pile deformation increases to the point that its foundation becomes instable and the pile-soil system is destroyed. The two test piles do

not experience the ultimate load simultaneously, so the test may end without the test pile resistance being completely destroyed.

The pile strain was determined here by embedding a steel sensor and concrete sensor in the pile, as mentioned above. The stress and bending moment distribution were calculated from the strain value as shown in Fig. 6-9.

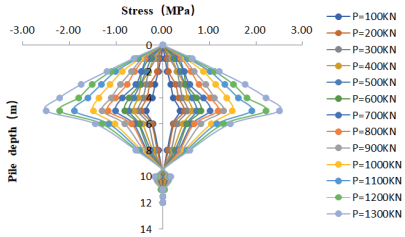

Fig. 6. Rebar compression and tension stress diagram of test pileI

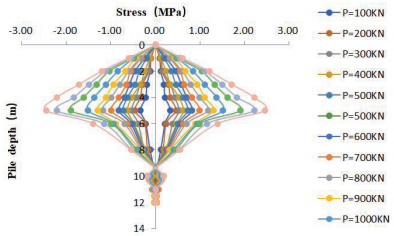

Fig. 7. Rebar compression and tension stress diagram of test pileII

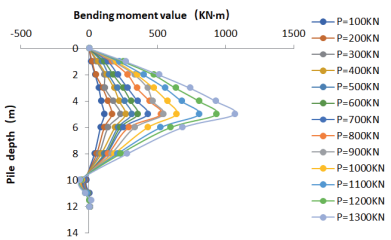

Fig. 8. Bending moment diagram of test pileI

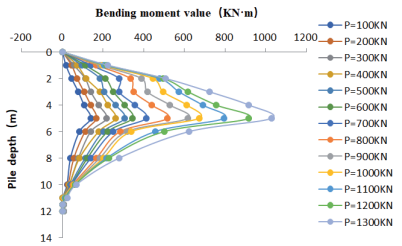

Fig. 9. Bending moment diagram of test pileII

As shown in Fig. 6 and Fig. 7, the stress on the pile head is relatively large as the upper soil pile side soil resistance is small and the degree of freedom is large. The displacement of the horizontal deflection curve of the soil layer is relatively large. The soil resistance of the pile side increases after entering the rock-socketed section, where the deflection curve displacement is relatively small. The maximum pile stress point moves slowly downward as the load increases. At the bottom pile end, the displacement of the deflection curve is a nearly reverse, minuscule value. The final positive and negative values alternate with the stress point 0. The rock-socked depth value of the pile foundation is approximately h=10. The overall force characteristics of the pile under the horizontal load can be determined based on these results.

As shown in Fig. 8 and Fig. 9, a bending moment distribution diagram of the pile was calculated from the strain values of the tested pile sections. The diagram shows the relationship between the pile horizontal load, the pile bending moment, and the pile sensor position. The load-bending moment

curve values of the two test piles are close to each other. The maximum bending moment was obtained from the top of the pile to the left and right positions 5-6 m from the pile. The strength of the rock layer is higher after this point and the bending moment value begins to decrease gradually. The bending moment produced by the two test piles around 8 m is already very small. A slight negative bending moment emerges close to the pile depth at 10 m (where the rock socket depth is about 6.0 m). This is at the point where the bending moment value reaches 0 for the first time, which is in the upper part of the rock layer. The bending moment of the pile increases as the load increases.

3. Finite element study of rock-socketed pile under horizontal load

3.1 Finite element model establishment

ABAQUS software was used to build a three-dimensional finite model and embed the pile foundation into the soil. The soil is divided into two parts, a soil layer and rock layer. Horizontal force was applied step-by-step on top of the pile foundation. The constitutive parameters of pile-soil-rock in the rock-socketed pile model were set according to actual engineering test geology and the pile foundation type. The total length of the rock-socketed pile in this case is 12 m, the sandy soil layer is 4.8 m above the rock layer, the rock layer is 7.2m., and the pile diameter is 2.2 m. The foundation soil surface layer is above a lower layer of moderately weathered rock. The total depth of the model foundation is 25.2 m. Horizontal loading was applied to the pile top in the test, so the digging depth was reserved for 0.8 m. The sand layer in the model is 4.0 m, the rock layer is 7.2 m, and the length and width of the foundation is 20×20 m. The pile-soil-rock material parameters are listed in Table 1.

Table 1. Pile-soil-rock material parameters

Pile-soil-rock material	Concrete strength	Deformation modulus	Poisson ratio	Internal friction angle	Expansion angle	Cohesion
Pile concrete	C40	$E_p = 3.25\times10^4\ Mpa$	$\mu_p = 0.20$	-------	-------	-------
Sand layer	-------	$E_S = 35 Mpa$	$\mu_S = 0.30$	25°	20°	-------
Moderately weathered rock	-------	$E_e = 1.2\times10^4\ Mpa$	$\mu_b = 0.31$	36°	3°	5.2kPa

In this model, the pile-soil-rock contact surface is a surface-to-surface contact element. Assuming that the pile-soil-rock interface has relative sliding, the behavior of pile-soil-rock under the working load was simulated as shown in Fig. 10.The friction coefficient between the pile and soil was set to

0.5 and the initial ground stress was 0.3MPa. The model was equipped with 13 levels of loading at the top of the pile; each level of load is 100kN totaling 1300kN.

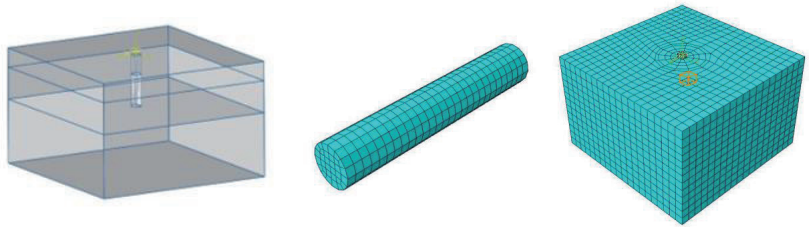

Fig. 10. Pile-soil overall grid division

3.2 Finite element calculation results

By obtaining the pile body stress curve of the model loaded at all levels, the bending moment values of each part of the pile were deduced as shown in Fig. 11 and Fig. 12.

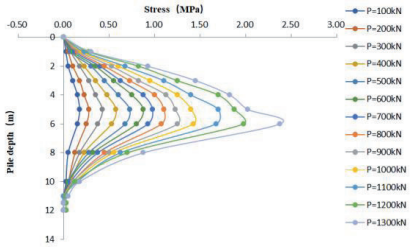

Fig. 11. Pile stress curve

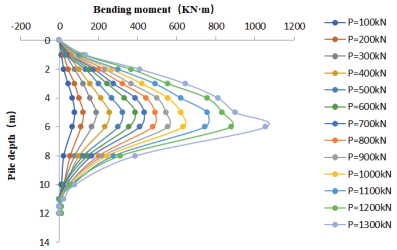

Fig. 12. Pile bending moment curve

At 0-5 m (pebble layer), the bending moment of the pile appears to increase to its maximum. The maximum bending moment value point (6 m) of the pile gradually moves downward as the load increases. The maximum bending moment value corresponds to the downward movement of the pile point by about 1 m. The bending moment of the pile tip is very small, which suggests that the bottom reinforcement ratio of the rock-socketed section is reduced.

The resistance of the soil around the pile is the most intuitive feedback of the normal stress generated by the pile-soil and pile-rock interface under the horizontal load. The normal stress of the pile-soil and rock interface was obtained by analyzing the distribution of the resistance of the soil along the pile, as shown in Fig. 13.

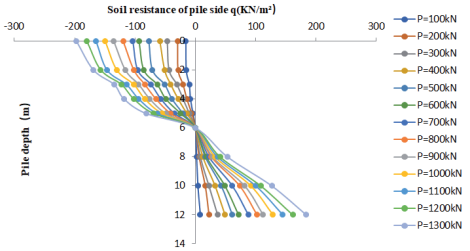

Fig. 13. Pile foundation resistance q distribution curve

The resistance value of the pile foundation soil at the 0 point appears between 5-6 m. The resistance of soil appears to reverse (contrary to the horizontal load direction) as the pile depth increases; it increases backward if it continues downward.

4. Theoretical analysis of rock-socketed pile depth

4.1 Embedded depth formula

The experiments and numerical simulation results show that under the action of horizontal force, the rock-socketed pile reaches the maximum bending moment at the pile depth of 3 H. After that, the strength of the rock layer increases and the bending moment value begins to decrease. A slight negative bending moment is generated at the pile depth of 6 H, which is the first time the bending moment value reaches 0. In terms of real-world force characteristics, the resistance of the rock mass at the side of the pile exist simultaneously. The following assumptions are imposed here regarding the embedded depth of rock-socketed piles.

(1) According to the finite element analysis results regarding soil resistance between the piles, when the rock-socketed pile rotates under the action of horizontal force, the rock mass resistance around the pile changes according to the cosine (Fig. 14);

(2) The distribution of the normal stress and shear stress on the side of the pile is proportional to the displacement and is distributed according to the sine (Fig. 15);

(3) The influence of the pile tip reaction is not considered.

(4) The rock-socketed pile bearing layer is impervious unaffected by erosion of the riverbed.

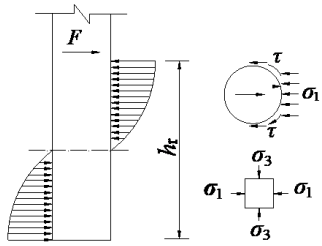

Fig. 14. Force mode of rock-socketed section and rock mass resistance beside pile

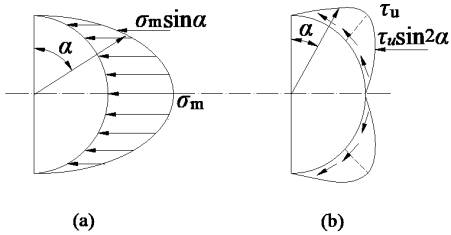

Fig. 15. Pile-rock lateral resistance distribution：(a) Normal resistance distribution (b) Lateral level friction distribution

According to the above assumptions and the static equilibrium conditions ($\sum M = 0$):

$$F \cdot h_r = 2\int_0^{h_r} P_u \cdot COS\frac{\pi \cdot x}{2h_r} \cdot (h_r - x)dx \tag{4.1}$$

and the solution is:

$$h_r = \frac{\pi^2 F}{8P_u} \tag{4.2}$$

where p_u is the ultimate resistance of the surrounding rock.

As shown in Fig. 15, the total ultimate resistance of the surrounding rock is composed of two parts: level friction and pile side normal resistance. Therefore, the ultimate resistance can be calculated as follows:

$$P_u = 2\int_0^{\pi/2} \frac{d}{2}\sigma_m \sin^2\alpha \mathrm{d}\alpha + 2\int_0^{\pi/2} \frac{d}{2}\tau_u \sin(2\alpha)\cos\alpha \mathrm{d}\alpha = \frac{\pi}{4}d\sigma_m + \frac{2}{3}d\tau_u \tag{4.3}$$

where σ_m is the maximum normal phase resistance in the rotation direction and τ_u is the ultimate level friction at the pile-rock interface, which can be obtained according to Coulomb's equation:

$$\tau_u = \sigma_m \tan\phi \tag{4.4}$$

Substituting Eq. (4.4) into Eq. (4.3) reveals the ultimate resistance of surrounding rock:

$$p_u = (\frac{\pi}{4} + \frac{2}{3}\tan\phi)d\sigma_m \tag{4.5}$$

Substituting the obtained ultimate resistance p_u of the surrounding rock into Eq. (4.2) allows the depth which ensures the rock-socketed pile is firmly embedded in the rock formation to be obtained:

$$h_r = \frac{\pi^2 \cdot F}{8(\frac{3\pi}{4} + \frac{2}{3}\tan\phi)d\sigma_m} = \frac{3\pi^2 \cdot F}{(18\pi + 16\tan\phi)d\sigma_m} \tag{4.6}$$

The comprehensive correction coefficient β can be 0.5-1.0. According to the lateral structure of the rock layer, the joint development may have a small or a large value.

$$h_r = \frac{3\pi^2 \cdot F}{(18\pi + 16\tan\phi)d\beta\sigma_m} \tag{4.7}$$

When h_r is determined, it must be ensured that the maximum lateral normal resistance $\sigma_{\max}$ of the surrounding rock does not exceed the allowable lateral resistance f_{rk} during lateral movement. That is:

$$[\sigma] = \frac{1}{K} f_{\mathrm{rk}} \tag{4.8}$$

where K is the safety factor, which is generally taken as 2.0; β is the comprehensive correction factor. Eq. (4.8) can be further simplified as follows:

$$h_r = \frac{6\pi^2 \cdot F_u}{(18\pi + 16\tan\phi) d \beta f_{rk}} \tag{4.9}$$

4.2 Comparative analysis of embedded depth theoretical formulas

The minimum rock-socketed depth in the test setup presented above was calculated to assess the rationality of the proposed theoretical formula. The pile diameter d was set to 2.2 m, the pile site was considered to be mainly weathered granulite with a gray-green, metamorphic structure, massive structure, and well-developed joints and cracks. Considering the development of rock $\beta = 0.5$, the allowable lateral resistance $f_{rk} = 3000kPa$ and the angle of the internal friction is 36°. The lateral normal resistance σ_m of the surrounding rock under the action of each class of load was input to Eq. (4.7) to determine the solid depth h_r of the rock-socketed pile embedded in the rock (Table 2).

Table 2. Depth h_r of rock-socketed piles under various loads

Graded load (kN)	100	200	300	400	500	600	700	800	900	1000	1100	1200	1300
Soil resistance (Kpa)	15.76	29.49	46.67	58.90	77.14	93.39	103.67	119.76	135.20	149.45	164.69	179.94	197.14
Embedded theoretical value (m)	5.51	5.89	5.58	5.89	5.63	5.58	5.86	5.80	5.78	5.81	5.80	5.79	5.72
h_r / d	2.50	2.68	2.54	2.68	2.56	2.53	2.66	2.64	2.63	2.64	2.64	2.63	2.60

Fig. 16 lists the ratios of rock-socketed pile embeded depth to pile diameter (ordinate) under different loads (abscissa). The theoretical correction value is 2.58, and the experimental and finite element analysis value is 2.7. Table 2 shows that the ratio of the buried depth of the rock-socketed pile to the pile diameter fluctuates significantly between 2.58-2.7 and its dispersion is small.

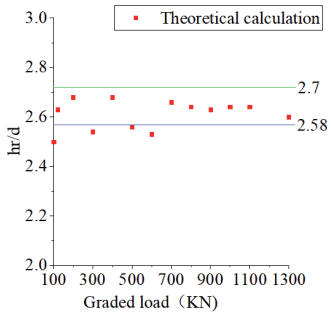

Fig. 16. Rock-socketed pile embedded depth h_r values under horizontal loads

5. Conclusion

A horizontal loading field test was conducted in this study followed by ABAQUS finite element simulations to study the horizontal bearing capacity of rock-socketed piles in bridge foundations. The strain of the pile and the stress state of the rock around the pile under various loads were determined to define the bending moment distribution law of the pile, as well as its stress and deformation mechanism. The finite element analysis results were compared against the experimental results, then utilized to establish a theoretical formula for the depth of large diameter rock-socketed piles embedded in bedrock. The conclusions can be summarized as follows.

(1) The length of the rock-socketed pile can be accurately determined via finite element analysis. Under the horizontal load, the bending moment zero (rock-socketed depth) of the pile is the most reasonable at 6.0 m when pile diameter is 2.2 m. The optimal depth of the rock-socketed pile is determined to be about 2.7 times the pile diameter.

(2) When the rock-socketed pile rotates under the action of horizontal force, the rock mass resistance around the pile changes according to the cosine. The distribution of normal resistance and level friction on the pile side is proportional to the displacement and distributed according to the sine. The effect of the pile tip reaction is not considered. The theoretical depth of the solid embedment of the rock-socketed pile in the rock layer is $h_r = \dfrac{3\pi^2 \times F}{(18\pi + 16\tan f)d\sigma_m}$.

(3) The lateral normal resistance of the surrounding rock in an actual bridge under the action of each class of load was substituted into the fixed depth formula to validate it. The solid depth of the rock-socketed pile was obtained. The discreteness is relatively small when $h_r = 2.58d$ (where d is the pile diameter). The theoretical results are in close agreement with field experiments and numerical

analysis. The proposed formula may thus provide a theoretical basis for the design of large-diameter rock-socketed pile embedded depth characteristics.

References

[1] C. H. Ghang, Q. H. Gao, C. Lou, "Model experimental study of rock rocketed pile in slope strata subjected to horizontal loading", Journal of Engineering Geology 27(2): 286-293, 2019.
[2] S. F. Guo, S. W. Qi, X. X. Li, Y. Zou, S. S. Zhang, "Strength and deformation characteristics of rock sample with discontinuities under numercial uniaxial compression simulation tests", Journal of Engineering Geology 24(5): 891-898, 2016.
[3] Z. Y. Liu, X. L. Jiang, H. Lin, "Numerical analysis for shear characteristic of soft structure plane with pile reinforcement", Journal of Central South University (Science and Technology) 42(5): 1461-1466, 2011.
[4] D. W. Wang, C. M. Wang, S. H. Kuang, "Selection and optimization of the site of bridge piled foundation on the layered rock slope", Journal of Engineering Geology 24: 861-867, 2016.
[5] H. J. Wang, D. A. Liu, Z. Q. Huang, G. X. Yuan, X. C. Li, J. R. Niu, Z. J. Zhao, X. S. Shi, "Mechanical properties and brittleness evaluation of layered shale rock", Journal of Engineering Geology 25(6): 1414-1423, 2017.
[6] W. D. Wang, J. B. Wu, S. B. Nie, "Field loading tests on large-diameter rock-socketed bored piles of Wuhan Greenland Center Tower", Chinese Journal of Geotechnical Engineering 37(11): 1945-1954, 2015.
[7] J. P. Jiang, G. Y. Gao, Y. S. Zhang, "Strengthening effect of total pile lateral friction by improving rock or soil strength at pile tip", Rock and Soil Mechanics 30(9): 2609-2615, 2009.
[8] C. Z. Gong, W. M. Gong, W. M. He, G. L. Dia, "Influence of Hole Side Roughness on Bearing Characteristic of Deep Rock-socketed Pile", China Journal of Highway and Transport 24(2): 56-61, 2011.
[9] M. H. Zhao, R. Y. Xia, P. B. Yin, C. W. Yang, Z. J. Xu, "Load transfer mechanism of socketed piles considering shear dilation effects of soft rock", Chinese Journal of Geotechnical Engineering 36(6): 1005-1011, 2014.
[10] H. F. Xing, M. H. Meng, W. Y. He, G. B. Ye, Z. K. Liu, "Distribution of shaft resistance of rock-socketed piles based on mechanical properties of pile-rock interface", Chinese Journal of Geotechnical Engineering 34(12):2220-2227, 2012.
[11] H. Mouzannar, M. Bost, M. Leroux, D. Virely, "Experi-mental study of the shear strength of bonded concrete-rock interfaces: surface morphology and scale effect," Rock. Mech. Rock. Eng., vol. 20, no. 1, pp. 1-25, Jun. 2017.
[12] H. M. Tian, W. Z. Chen, D. S. Yang, "Experimental and numerical analysis of the shear behaviour of cemented concrete-rock joints", Rock Mechanics and Rock Engineering 2017(1):1-25, 2015.
[13] C. Liu, Q. Hu, Y. Wang, S. M. Zhang, "In-Plane Stability of Concrete-Filled Steel Tubular Parabolic Truss Arches", International Journal of Steel Structures 18(4): 1-12, 2018.
[14] A. Kilic, E. Yasar, A. G. Celik, "Effect of grout properties on the pull-out load capacity of fully grouted rock bolt", Tunneling and Underground Space Technology 17(4):355-362, 2002.
[15] Y. Geng, G. Ranzi, Y. T. Wang, Y. Y. Wang, "Out-of-plane creep buckling analysis on slender concrete-filled steel tubular arches", Journal of Constructional Steel Research 140: 174-190, 2018.
[16] J. P. Seidel, C. M. Haberfield, "A theoretical model for rock joints subjected to constant normal stiffness direct shear", International Journal of Rock Mechanics and Mining Sciences 39(5):539-553, 2002.
[17] H. S. Zhang, Y. Y. Wang, "Structural mechanics analysis on coexistent cable support system during system transformation from cable-stayed to suspension", China Civil Engineering Journal 51(10): 88-96, 2018.
[18] S. Hoonil, J. Sangseom, C. Chunwhan, "Shear load transfer for rock-rocketed drilled shafts based on borehole roughness and geological strength index", International Journal of Rock Mechanics and Mining Sciences 45:848-861, 2008.
[19] C. Liu, Y. Wang, X. Wu, S. Zhang, "In-Plane Stability of Fixed Concrete-Filled Steel Tubular Parabolic Arches under Combined Bending and Compression", Journal of Bridge Engineering 22(2): 04016116.1-04016116.15, 2016.
[20] X. F. Gu, C. M. Haberfield, "Laboratory investigation of shaft resistance for piles socketed in basalt", International Journal of Rock Mechanics and Mining Sciences 41(3): 465-471, 2004.
[21] L. H. Han, T. M. Mu, F. C. Wang, B. K. Fan, W. Li, J. Liang, C. Hou, "Design theory of CFST (concrete-filled steel tubular) mixed structures and its applications in bridge engineering", China Civil Engineering Journal 53(5): 1-24, 2020.
[22] M. G. Zertsalov, D. S. Konyukhov, "Analysis of piles in rock", Soil Mechanics and Foundation Engineering 44(1): 9-14, 2007.

Received: 23.12.2020, Revised: 18.03.2021